On the Persistence of Geomagnetic Flux Lobes in Global Holocene Field Models

Monika Korte, Richard Holme

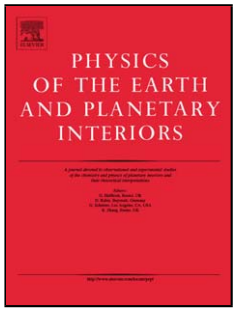

Title: On the Persistence of Geomagnetic Flux Lobes in Global Holocene Field Models

Authors: Monika Korte, Richard Holme

PII: S0031-9201(10)00160-3
DOI: doi:10.1016/j.pepi.2010.08.006
Reference: PEPI 5325

To appear in: *Physics of the Earth and Planetary Interiors*

Received date: 12-1-2010
Revised date: 9-8-2010
Accepted date: 17-8-2010

Please cite this article as: Korte, M., Holme, R., On the Persistence of Geomagnetic Flux Lobes in Global Holocene Field Models, *Physics of the Earth and Planetary Interiors* (2010), doi:10.1016/j.pepi.2010.08.006

On the Persistence of Geomagnetic Flux Lobes in Global Holocene Field Models

Monika Korte[a], Richard Holme[b]

[a]*Helmholtz Zentrum Potsdam, Deutsches GeoForschungsZentrum GFZ, Telegrafenberg, 14473 Potsdam, Germany*
[b]*School of Environmental Sciences, University of Liverpool, Liverpool, L69 3GP, UK*

Abstract

To investigate the longevity and robustness of high-latitude flux patches in the geomagnetic field at the core-mantle boundary, we present time-dependent models of the geomagnetic field for the past 7000 years. Our models use the same data set as previously used for time-dependent archaeomagnetic field modelling, but constrained with additional *priori* models from time averages of field models covering the last 150, 400 and 3000 years. We find that the data are consistent with flux patches existing in both north and south hemispheres for the past 7000 years, and that the northern hemisphere patches at least have highly dynamic behaviour. Simple averaging of the historical field may not be appropriate to obtain a characteristic time-averaged model of the field for comparison with other geophysical observables. Our results should inform geodynamo studies of thermal core-mantle coupling, and of possible long-term structure in the geomagnetic field.

Key words: Geomagnetism, flux lobes, archaeomagnetic field, time-averaged field, millenial secular variation.

1. Introduction

Near-surface observations of the geomagnetic field provide a powerful probe of the dynamics of the top of the Earth's core, and ultimately of the whole geodynamo. Models of the core surface field have been constructed on a wide range of time scales, from recent, high-resolution models from satellite data (e.g. Lesur et al., 2008; Olsen et al., 2009), through time-dependent models of the historical (Jackson et al., 2000) and archaeomagnetic

field (e.g. Korte and Constable, 2005; Korte et al., 2009), to time-averaged models of the last 5 Myr paleomagnetic field (e.g., Johnson and Constable, 1995; Kelly and Gubbins, 1997). As the time periods increase, data quality and distribution decrease, leading to models with lower resolution in both space and time. Nevertheless, there is evidence of coherent structure in the field on all time scales; such structure is highly significant, and has been interpreted in terms of mantle control on the geodynamo, through thermal (Bloxham and Gubbins, 1987) or possibly electromagnetic (Holme, 2000) core-mantle coupling. Two features of the field have been of particular interest: low secular variation under the Pacific hemisphere, and stationary flux lobes at high latitudes, possibly in symmetric locations in the northern and southern hemisphere. It is on the latter patterns that this paper focuses.

Figure 1 shows the time-averaged field structure at the core-mantle boundary (CMB) on four time scales: the historical period from 1840 – 1990 (for which detailed dedicated observations are available, in particular including absolute magnetic intensity determinations, and time-evolution of the field from magnetic observatories), the longer historical period from 1590 – 1990 (prior to 1840 dominated by data from ship's logs (Jonkers et al., 2003)), the archaeomagnetic field for the past 3000 years (inclucing many sedimentary records), and for the past 7000 years. Comparison of the averages shows the expected reduction in resolution with averaging time, particularly in the southern hemisphere. All the averaged global models predict the existence of two or three lobes of strongest magnetic flux in the Northern hemisphere (Bloxham et al., 1989), with similar features observed in longer term time-averaged global models based on paleomagnetic data from the past 5 million years (Johnson and Constable, 1995; Kelly and Gubbins, 1997). However, the southern hemisphere flux patches, clear in recent historical and satellite models, are not seen in the older models.

It is difficult to decide how much field structure we can expect to resolve with archaeo- and paleomagnetic data, where data and dating uncertainties are high and often not well-understood. Simply truncating the spherical harmonic expansion avoids any small-scale structure, but may map higher degree energy into the lower degree model coefficients. Instead, we seek regularised models: models that both fit the data, and also minimise some

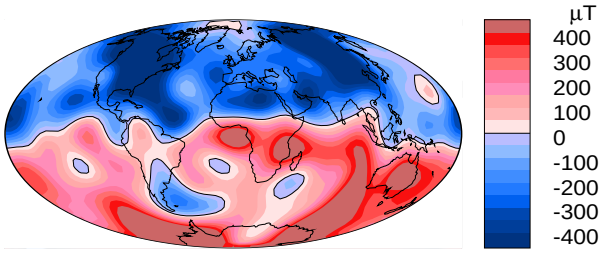

(a) gufm1 Br 1840 AD - 1950 AD

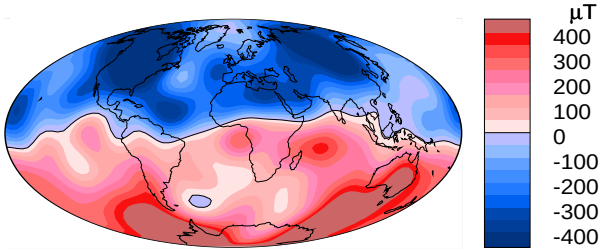

(b) gufm1 Br 1590 AD - 1990 AD

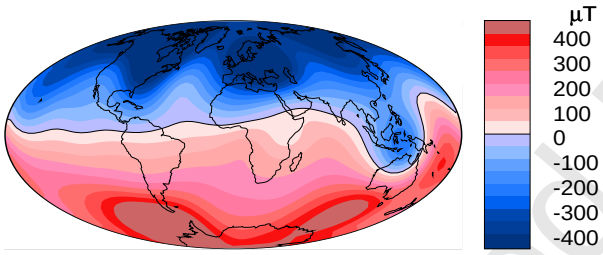

(c) CALS3k.3 Br 1000 BC - 1990 AD

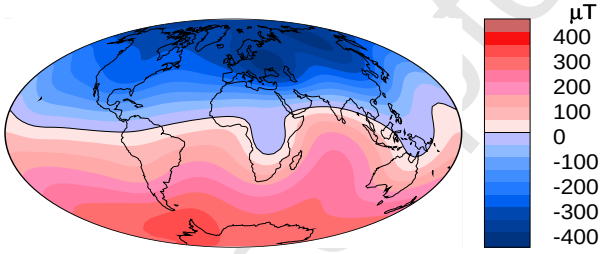

(d) CALS7K.2 Br 5000 BC - 1950 AD

Figure 1: Time averaged radial field component at the core-mantle boundary of the three a priori models and CALS7K.2. (a) and (b) are 150 and 400 year averages, respectively, of *gufm1* by Jackson et al. (2000), (c) and (d) are the overall time averages of CALS3k.3 (Korte et al., 2009) and CALS7K.2 (Korte and Constable, 2005), respectively. Northern hemisphere flux patches are seen at high latitudes under North America and Siberia, and in the more recent models approximately symmetric southern counterparts are seen south of South America and Australia.

physical quantity, such as a bound on the electrical dissipation in the dynamo (Gubbins, 1975), the mean square field strength over the CMB, or its time variability. Such assumptions bias the solution for the magnetic field towards the minimum magnitude capable of explaining the observations, and therefore provide a lower bound for the true field strength or complexity. Formally (in a Bayesian sense) we are seeking a model which fits the data, subject to an *a priori* model of zero magnitude – that there is no field! This assumption is clearly not reasonable: the Holocene data clearly indicate the existence of a persistent field. More specifically, if a time-dependent field model of the archaeomagnetic field suggests episodic flux patches in the north, and none at all in the south, is this because the data demonstrate that the flux patches are not there at some times, or because the model is biased towards low magnitudes, and with limited data, the flux patches are eliminated to reduce the field strength, even (possibly) at the cost of worsened fit to data?

To investigate this issue, we seek models of the field which minimise the deviation of the time-dependent model from a time-averaged model of the field from more recent times, in which the flux patches are seen clearly. Philosphically, an *a priori* model of a field like that of the present day seems no more unreasonable than a zero prior, which we know to be false. By doing this, we investigate whether it is the data or the regularising assumptions which lead to episodic or missing flux patches. If the models we generate include the flux patches, then we can argue that there is insufficient evidence to reject the patches being consistent features in the field; if the patches move around, are episodic or absent, then we may reject this hypothesis, and make stronger statements about the behaviour of the centenial and millenial structure of the geomagnetic field.

2. Data and a priori models

The data set is the one used to generate CALS7K.2 (Korte and Constable, 2005), which is readily available from the EarthRef Digital Archive (http://www.earthref.org) (Korte et al., 2005). It consists of directional data from archaeomagnetic studies and lake sediment records, and intensity data determined from archaeological artefacts and lavas. We realize that additional data have been published meanwhile, but in order to allow for a comparison

to the CALS7K.2 model we retained that data compilation for this study. An iterative data rejection scheme was used in devising CALS7K.2, and we consider only the final data set of 27067 values. All data which could not be fit within two average standard deviations by a first model had been rejected in this dataset (see Korte and Constable, 2005).

The choice of the prior model is not straightforward. It is not clear over how long a time interval the field has to be averaged in order to minimise rapidly varing small-scale structure to represent properly only persistent larger-scale features. Average over too short a time period, and rapidly varying features are mapped into the stationary mean model; over too long a period and we lose structure due to inadequate data distribution or quality. **In order not to make unnecessary assumptions about amount and position of persistent structure we consider three** *a priori* **models based on data and without additional filtering:** *gufm1* (Jackson et al., 2000) averaged over the time intervals 1840 to 1990 and 1590 to 1990, and the time-average of the recently published 3kyr model CALS3k.3 (Korte et al., 2009). **All of these averaged models clearly show two pairs of flux lobes, which are approximately hemispherically symmetric. As testing the compatibility of southern hemisphere flux lobes with the 7kyr data set is one of our main motivations, we did not include any longer-term averaged models, which do not show a similarly clear pattern.** The motivation for considering *gufm1* time averages over both 150 and the full 400 years is twofold: First, 150 years is of the order of the temporal resolution of CALS7K.2 (Korte and Constable, 2008). Second, the spatial resolution of this model clearly increases with time as the number and quality of available data increases. In particular, 1840 dates the establishment of geomagnetic observatories, and also start of widespread measurement of absolute intensity. The 150 year average is consequently of higher resolution, containing more smaller scale structure; however, some of this may be present because of insufficient averaging (Fig. 1a and b). The intensity of the model prior to 1840 is unconstrained by data (defined only by a backwards-extrapolation of the dipole strength, cite[]jackson00); this is assumed to be sufficiently close to the real behaviour not to overly bias the average model structure. The *gufm1* model is calculated to spherical harmonic degree and order

14; we simply truncated the time-average at degree and order 10 to match the expansion limit of our new models, **which seems justified by the fact that with reasonable regularization all the new models show less power than their priors in spherical harmonic degrees of eight and higher**.

The CALS3k.3 model is based on an updated archaeomagnetic and sediment dataset (Donadini et al., 2009) and spans the time 1000 BC to 1990 AD. Both spatial and temporal resolution are somewhat higher than for CALS7K.2. The time average (Fig. 1c) contains significantly less structure than the historical averages, but does show clear flux lobes in both the northern and southern hemispheres similar to those seen in the *gufm1* averages.

3. Four new models

The modelling method is basically the same as used for the *gufm1* (Jackson et al., 2000) and CALS7K.2 (Korte and Constable, 2005) models and is described in detail there. The basis functions for the inversion are spherical harmonic functions in space with individual coefficients expanded in cubic B-splines in time to provide a continuous description (Bloxham and Jackson, 1992). Maximum spatial and temporal resolution provided by the basis functions are higher than the actual resolution considered feasible from the data with their uncertainties and inhomogeneous global distribution. Regularisations in both time and space are applied in order to find models with minimum structure required by the data. Many different models may be appropriate solutions to the inverse problem, ranging from very smooth models with large misfit to the data to complex models fitting the data closely. The regularisation parameters (the damping parameters or Lagrange multipliers controlling the relative penalty assigned to data misfit and model complexity) for the preferred model are commonly found either from the "knee" of a curve trading off misfit against roughness, or by fitting the data to the tolerance given by the uncertainty estimates of the data. For long-term magnetic field models comparisons of resulting time-averaged main field and secular variation geomagnetic power spectra to models constructed with historical data also seem suitable criteria, as higher average spatial or temporal complexity, i.e. higher power in spherical degrees with the exception of 1 and perhaps 2 and 3, is extremely

unlikely and certainly not resolvable with the presently available amount and quality of Holocene data (Korte and Constable, 2008). **The chosen regularistion norms result in a damping of power in main field and secular variation that increases for higher SH degrees, so that small scale / short term structure are efficiently suppressed if the applied regularisation factors result in comparable spectral values for the low degrees (Korte et al., 2009).**

In this study, however, we do not seek an absolute minimum structure model, but the minimum deviation from a given average field structure required by the data. We replace the constraint of minimising a bound on Ohmic dissipation necessary in the dynamo to generate the observed field (Gubbins, 1975), which was used as spatial regularisation for both *gufm1* and CALS7K.2, with minimising the radial field deviation at the CMB from an *a priori* model, i.e. the quantity

$$S(\mathbf{m}_0) = \int_{CMB} \left(B_r - B_r(\mathbf{m}_0)\right)^2 d\Omega, \tag{1}$$

where B_r is the radial field of the new model and $B_r(\mathbf{m}_0)$ that of the *a priori* model $\mathbf{m}_0$. The integration is performed over solid angle $d\Omega$ at the core surface, averaged over the time period of the model. This condition is easily expressed as a quadratic norm of the geomagnetic Gauss coefficients; we minimise

$$\sum_{l=1}^{l_{\max}} \frac{(l+1)^2}{2l+1} \left(\frac{a}{c}\right)^{2l+4} \sum_{m=1}^{l} \left[(g_l^m - g_l^m(\mathbf{m}_0))^2 + (h_l^m - h_l^m(\mathbf{m}_0))^2\right] \tag{2}$$

where a is the radius of the Earth, c the radius of the CMB, $\{g_l^m, h_l^m\}$ are the geomagnetic Gauss coefficients of spherical harmonic degree l and order m, and $\{g_l^m(\mathbf{m}_0), h_l^m(\mathbf{m}_0)\}$ the coefficients of the *a priori* model.

Studies of virtual axial dipole moment (McElhinny and Senanayake, 1982; Yang et al., 2000) and the previous millennial scale models indicate that the dipole moment has varied significantly over the past 7 kyrs. The dipole is the strongest field contribution; we were concerned that taking it into account in investigating the required deviation might have a dominating influence. Therefore, we also tested models where either the axial dipole coefficient, or all three dipole coefficients were not influenced by the spatial regularisation.

We found that with our criteria for the preferred amount of regularization the differences between these three types of model were small. Nevertheless we retained only the models where the dipole was not included in the spatial regularization in the following comparison.

The final modelling procedure minimises the functional

$$\mathrm{RMS}^2 + \lambda_S S(\mathbf{m}_0) + \lambda_T T \tag{3}$$

with spatial and temporal damping factors (Lagrange multipliers) λ_S and λ_T respectively. The normalised root mean square misfit (RMS) between model predictions $\hat{x}_i$ and data x_i is defined as

$$RMS = \sqrt{\frac{1}{N}\sum_{i=1}^{N}\left(\frac{x_i - \hat{x}_i}{\sigma_i}\right)^2}, \tag{4}$$

with uncertainty estimates σ_i and N the number of data. The spatial norm compared with the *a priori* model $\mathbf{m}_0$ is defined in equation (1), and the temporal norm (like the spatial norm, averaged over the modelling period) is defined

$$T = \int \left(\frac{\partial^2 B_r}{\partial t^2}\right)^2 d\Omega. \tag{5}$$

(t is time) which can be calculated using a quadratic norm of the form of equation (2).

In the end we calculated four new models, summarized in tabletab:models. For comparability, we first reconstructed a model M0 similar to CALS7K.2 with zero prior model, but regularising by minimising the mean square radial field at the CMB instead of Ohmic dissipation norm, and also excluding the dipole coefficients from the regularization. We chose the damping factors such that the resulting model shows similar main field and secular variation spectra to CALS7K.2 and has a comparable data misfit – the values are $\lambda_S = 5 \times 10^{-11}$ and $\lambda_T = 10^2$. Three further models were constructed with the same damping parameters; the only difference being the *a priori* model. The averaged 150 and 400 year *gufm1* were used respectively for models M150 and M400. CALS3k.3 was the prior model for M3k.

Table 1: The four new models and their priors.

Model	Prior
M0	0
M150	*gumf1* averaged from 1840 to 1990
M400	*gufm1* averaged from 1590 to 1990
M3k	CALS3k.3 averaged over 3kyr

4. Results

As a first step to comparing our models, Figure 2 shows the main field and secular variation spectra of the time averages of the four investigated models at the CMB together with the spectra of the *a priori* models and the CALS7K.2 spectra. By plotting these spectra at the CMB we emphasize the differences in higher degrees. The secular variation spectra of the four new models look nearly identical, **which is not surprising due to the common temporal damping applied independently from the spatial damping.** The time-averaged spectra of the new models clearly resemble those of their respective *a priori* models, except in the case of M0 which was designed to be similar to CALS7K.2. The increasing deviation with spherical harmonic degree above degree $l = 5$ between M0 and CALS7K.2 is due to the different regulariation applied.

We next consider global diagnostics averaged over the whole 7 kyr time interval. We calculate the RMS misfit (equation 4), departure from *a priori* model $S(\mathbf{m}_0)$ (equation 1) and temporal norm T (equation 5). We also consider the overall spatial structure $S(0)$

$$S(0) = \int_{CMB} B_r^2 d\Omega. \tag{6}$$

For M0, with the zero *a priori* model, we obviously have $S(\mathbf{m}_0) = S(0)$. These diagnostics are given in Table 2. (Note that although the dipole terms are excluded from the damping, all of the norm calculations include the dipole components to give quantities that have direct physical meaning.) The dependence of overall model complexity on the *a priori* model is quantified by the values of $S(0)$, characterising the overall average model complexity; this measure is higher by 29% for M150 than for M0. All data included in the investigated

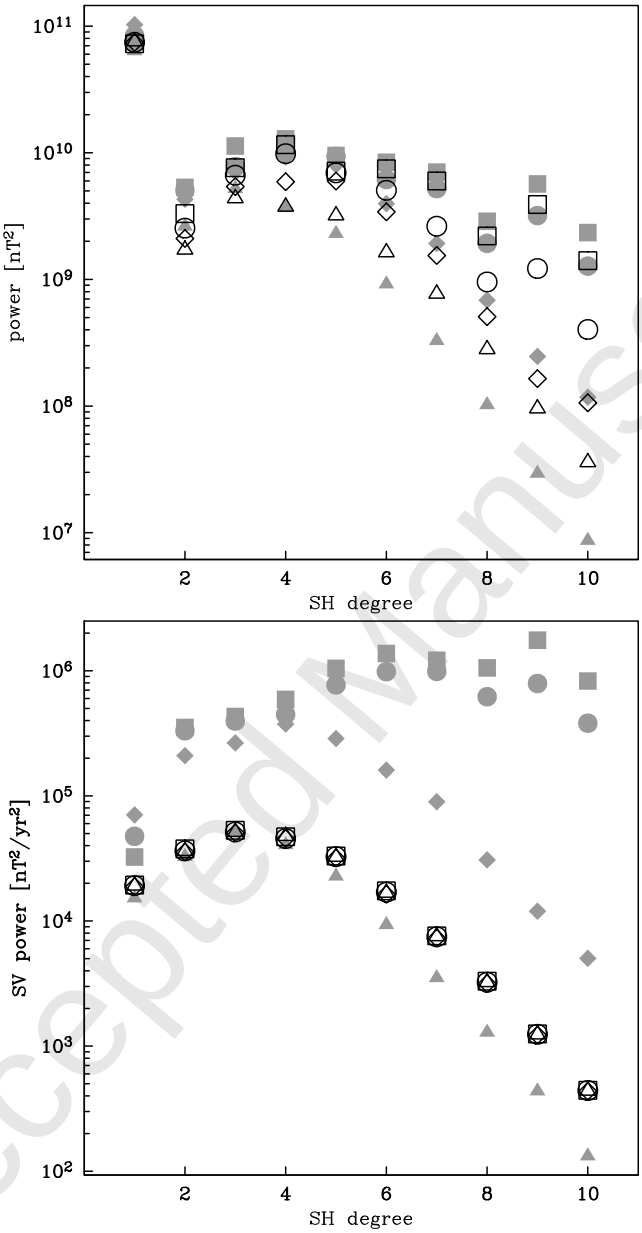

Figure 2: Time averaged main field (top) and secular variation (bottom) geomagnetic power spectra at the core-mantle boundary for models M0 (open triangles), M150 (open squares), M400 (open circles), M3k (open diamonds) and time averaged *gufm1* for 1840 to 1990 (gray squares), 1590 to 1990 (gray circles), CALS3k.3 (gray diamonds) and CALS7K.2 for 5000 BC to 1950 AD (gray triangles).

Table 2: Rms misfit and spatial and temporal complexity of new models

Model	rms	T (nT^2yr^{-4})	$S(0)$ (nT^2)	$S(\mathbf{m_0})$ (nT^2)
Time interval 5000 BC to 1950 AD:				
M0	0.989	10.69	5.9×10^{10}	5.9×10^{10}
M150	0.997	10.85	7.6×10^{10}	2.0×10^{10}
M400	0.990	10.63	7.0×10^{10}	1.6×10^{10}
M3k	0.984	10.53	6.3×10^{10}	1.2×10^{10}
Time interval 5000 BC to 1000 BC:				
M0	0.968	7.87	4.8×10^{10}	4.8×10^{10}
M150	0.975	7.94	6.6×10^{10}	3.0×10^{10}
M400	0.961	7.62	6.0×10^{10}	2.3×10^{10}
M3k	0.956	7.49	5.3×10^{10}	1.6×10^{10}

dataset for the time interval 1000 BC to 1950 AD form a subset of the data used in the construction of CALS3k.3, the a priori model for M3k. This will inevitably give a bias in our results; the time-averaged CALS3K model is bound to be a good fit to the CALS7K data set for the period after 1000 BC. To accommodate this bias, we calculate two sets of diagnostics in table 2, first for the whole 7000 years, and secondly separately for the time interval 5000 BC to 1000 BC, which is not considered in any of the a priori models. This second set of diagnostics should eliminate (or at least limit) the bias from considering common data sets. With so many diagnostics of the models presented, it could be extremely difficult to determine which **prior model is most compatible with the observations**; however, fortunately, the results obtained allow a clear ranking of the models. Comparing the three models with time-averaged *a priori* model, all four diagnostics (misfit, temporal norm, absolute spatial norm and departure from *a priori* model) are largest for M150, intermediate for M400, and smallest for M3k; this ordering applies both for the full time interval and also for the first 4000 years. Comparing with M0, the model with a zero prior (the standard damping), all the other models have more spatial power (as would be expected). Comparing misfit and temporal norm, the M150 model performs less well than

M0, the M400 marginally better, and the M3k substantially better.

In conclusion, the data can be fit better by a model requiring less temporal variability if a suitable *a priori* model is used. Among the a priori models tested the averaged CALS3k.3 turns out to be the most suitable, with relatively little deviation required, yet giving the best fit to the data and least required temporal variation. The data are least compatible with *gufm1* averaged only over the most recent 150 years.

A more detailed analysis of the behaviour of the solution norms as a function of time is provided in Fig. 3, which plots the mean square radial field, the mean square departure of the field from the *a priori* model, and the temporal norm as a function of time. The profiles for the different *a priori* models are generally similar, especially for the temporal complexity T. The absolute amount of complexity, $S(0)$, shows nearly identical relative variations with time. The relative deviation from the three non-zero *a priori* models also is similar, with maximum values around 4000 BC for all, and again between 0 and 1000 AD for the two *gufm1* a priori models.

The average spatial structure of the models is shown by plots of their mean radial field at the CMB (Fig. 4). The averages of the different models show clear similarities in large-scale features, while reflecting the amount of complexity of the a priori model (for example, the small near-equatorial flux patches in M150 are clearly a result of insufficient time-averaging of the *a priori* model in this region). The available data are clearly compatible with two southern hemisphere flux lobes which are persistent enough to show up in the time-averaged model. In all four models, there are three (rather than two) flux lobes present in the northern hemisphere, despite the prior model for M150 and M400 requiring only the two lobes seen in today's field. We may therefore be confident that the Holocene data do require a third northern flux lobe under Europe. A similar flux lobe pattern could also exist in the southern hemisphere, but none of the prior models show this feature, and there are insufficient data to constrain this question. **Note, however, that even recent high-resolution field models for one epoch, like e.g. the IGRF for 2005 (Macmillan and Maus, 2005), show a somewhat similar third flux lobe if truncated at spherical harmonic degree 5 or 6 (with counterpart in the southern**

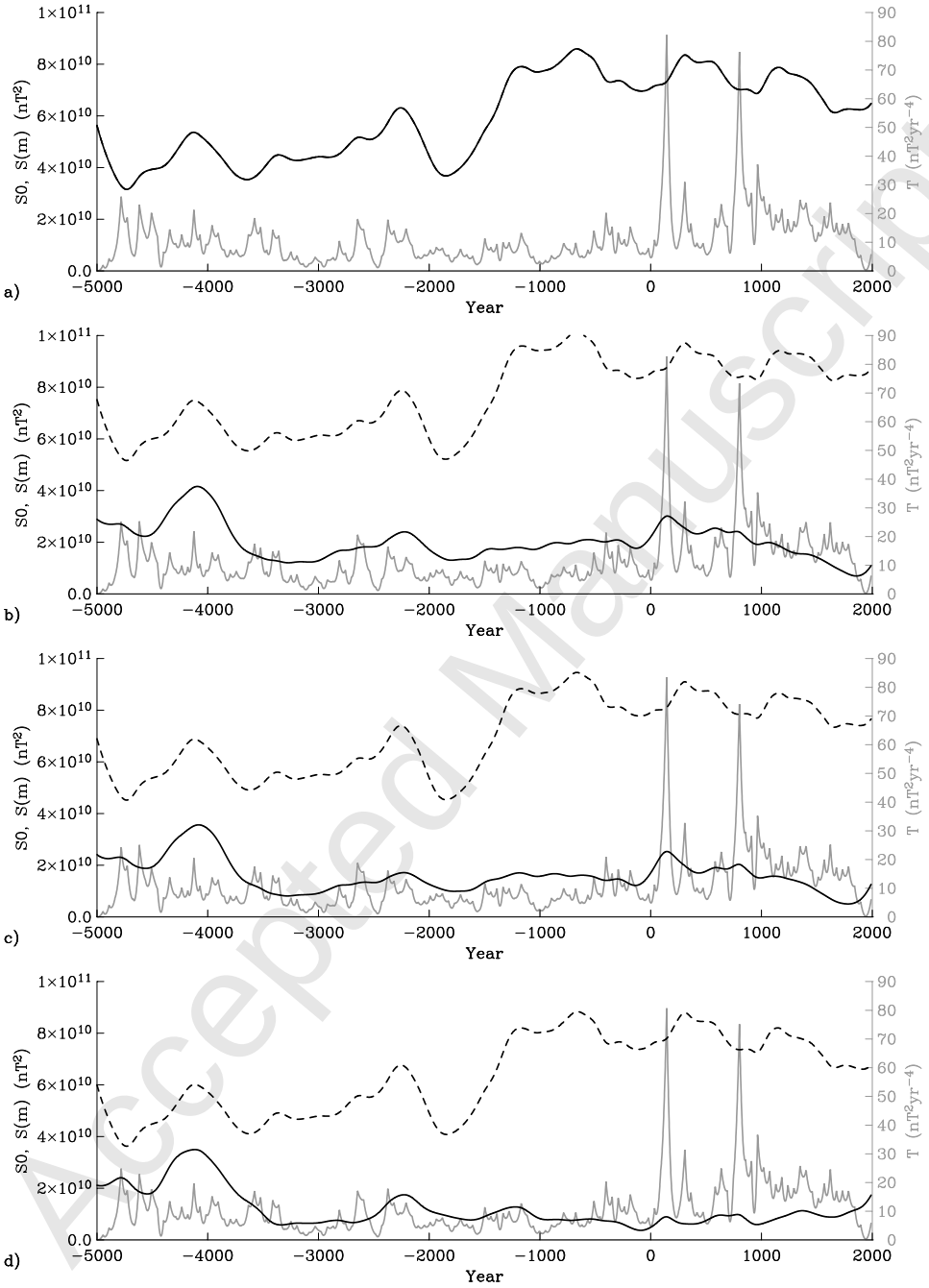

Figure 3: Spatial and temporal complexity as measured by $S(\mathbf{m_0})$ (black solid line), $S(0)$ (dashed line) and T (gray) for models a) M0, b) M150, c) M400, d) M3k. The solid and dashed lines are by definition identical for M0.

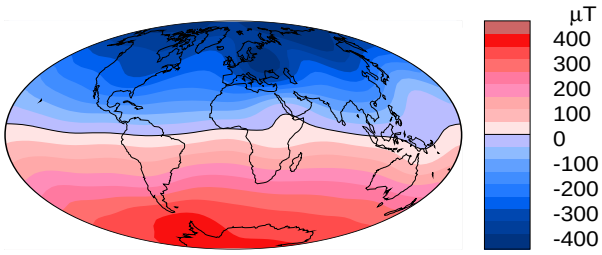

(a) M0 Br 5000 BC - 1950 AD

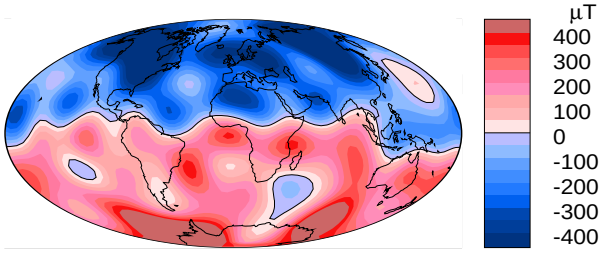

(b) M150 Br 5000 BC - 1950 AD

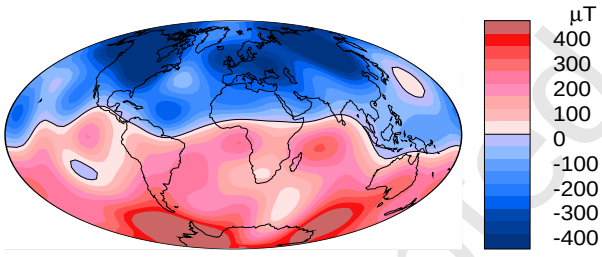

(c) M400 Br 5000 BC - 1950 AD

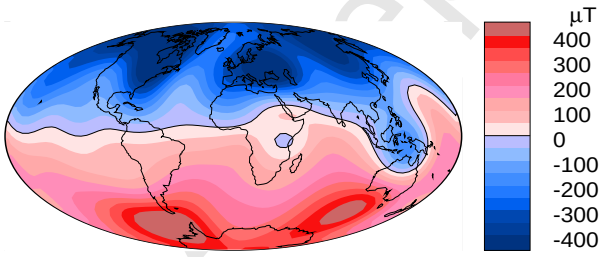

(d) M3k Br 5000 BC - 1950 AD

Figure 4: Time averaged radial field component at the core-mantle boundary of the four new models.

hemisphere). This apparent third flux lobe therefore might be a manifestation of unresolved but non-averaging smaller scale structure. Another common feature of all models is an area of positive radial field in the north-western Pacific, although its detailed form and strength is affected by the different prior models. This feature has also been seen in previous models (see, for example, the snapshot models of Constable et al. (2000)), and shows up clearly in longer time-period palaeomagnetic models (for example, Johnson and Constable, 1997).

Animations of the evolution radial field are provided in Fig. 5 (electronic version or supplemental material) with the present position of flux lobes outlined by the +/-400 μT isolines of the 400 yr time-averaged *gufm1* model. These animations show substantial variability of the flux concentrations on multi-centennial time-scales in all four models, confirming that they are in fact required by the data and with only minor influence from the choice of *a priori* model. Despite a large amount of movement and/or decrease and increase of flux, the flux concentration is rather high most of the time in the area of the present North American flux lobe, with only two time intervals of significantly weaker flux spanning about 500 years around 1950 BC and 650 AD. Similarly, the flux concentration remains high in the area of the present Siberian flux lobe except for 200 to 600 year intervals around 3450 BC, 1800 BC and 100 BC. Significantly stronger flux than present, however, appears in the European region for 2 to 5 centuries around 5000 BC, 4500 BC, 2500 BC, 1500 BC, 250 BC and 800 AD. Flux variations are weaker in the southern hemisphere, likely as a consequence of the sparcity of southern hemisphere data.

5. Discussion

Our primary result is clear and perhaps unsurprising: southern hemisphere flux patches are consistent with the available data. There is no evidence requiring that they are less persistent then their northern hemisphere counterparts. However, some interesting further results emerge from more detailed comparisons. Constraining the model about the 150 year time average is apparantly less appropriate than applying no constraint at all. This suggests that, although tempting because of the much higher quality data for this period, using this

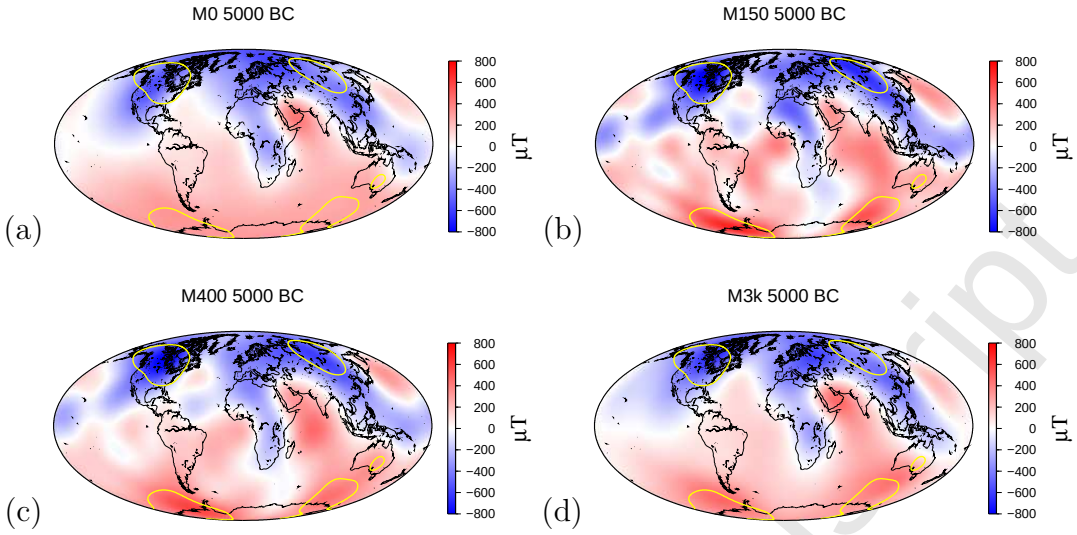

Figure 5: Animations (electronic version or supplemental material) of the radial magnetic field evolution of models (a) M0, (b) M150, (c) M400 and (d) M3k at the CMB. Yellow lines indicate the +/-400 μT contour lines of the 400 yr time averaged *gufm1* model.

time average as a proxy for long-term field behaviour is not appropriate. Why might this be? One possibility is that the averaging time is insufficient to average out small scale motions (for example, the propagation of flux patches along the equator (Jackson, 2003)), leaving small scale features to be fit that are not persistent on longer time scales. Another important effect is likely to be the appearance after 1840 of the southern hemisphere reversed flux patch, associated by Gubbins (1987) with the current rapid decay of the axial dipole field. A third effect is that the particularly strong flux lobes from the *a priori* model for M150 act to preclude the variability in the position of the northern hemisphere flux lobes; from examination of the movie, there is certainly evidence that the prior model is having a strong influence on the position and longevity of these features compared with the other three models. Any or all of these explanations suggest that if we wish to correlate geomagnetic field morphology with other geophysical observables (e.g. geoid, seismic tomography), then the recent historical field or even high-resolution models of the current field from satellite data may be less appropriate than the longer term averages.

It is interesting to note that all three models using *a priori* field averages for regularization cleary indicate the existence of three large northern hemisphere areas of high flux

concentration on average (Fig. 4), while the historical field averages (and present field) mainly show two (Fig. 1). The highly dynamic evolution of the flux pattern over time, however, makes it difficult to clearly distinguish between lateral movements of flux patches and growth and decay of regional flux concentrations. Interestingly, a strong appearance of all three flux patches simultaneously is rare. Their movement with time is also significant, because the prior models (M150 in particular) favour restraining them to a single location; that they are nonetheless variable in their positions suggests that this is a true feature of the field required by the data. Nevertheless, the dynamic nature of the flux patches has important implications for numerical dynamo studies of thermal core-mantle example. For example, in their dynamo calculations, Willis et al. (2007) have **located a region of parameter space (admittedly far from Earth-like)** in which a numerical dynamo code yields flux lobe patterns similar to field observed for the present day. These patches are dynamic, moving around and occasionally dividing, but none the less, apparantly less dynamic than the behaviour implied by the observations and our modelling here. Additional study (Davies et al., 2008) has located a parameter regime with evidence of the three-fold symmetry we observe in our models; **our models suggest that an evaluation of the transition between these two regimes would be of great interest**. No corresponding southern hemisphere counterpart for the third flux lobe centered under Europe appears. This is not surprising as our a priori models do not encourage this, and the southern hemisphere data are sparse. However, the three models do suggest a region of weak to reversed flux under southern Africa and surrounding areas, roughly the same region as the present day Southern Atlantic Anomaly (Gubbins and Bloxham, 1985). Together with the appearance of a strong reverse flux patch around Southern Africa in the first two millennia of the models, this **might be interpreted as** a preferred area for the recurrence of significant reverse flux and consequently minimum field strength. However, this southern hemisphere feature results from the strong inclination variation seen in one African sediment record between 4000 and 5000 BC (Lake Victoria by Mothersill (1996)). The reverse flux area south of the equator seen in the averages in Fig. 4 disappears if this specific sediment record is omitted from the modelling. To our knowledge there are to

date no data to the south of that location between Argentina and Australia to support or contradict the strong effect of these data on the model. Until such data are available this model feature should be regarded with caution.

6. Conclusions

We have investigated persistent structure in the time-averaged geomagnetic field on time-scales from centuries to millennia. The deviation from different time-averaged field models has been used as regularization constraint for spatial structure in modelling the 7kyr dataset which had previously been used for the CALS7K.2 model. Comparisons of misfit and temporal variability resulting with fixed modelling parameters show that the data are less compatible with field averages of the past 150 or 400 years than with a 3kyr average. This indicates that small-scale structure present in field averages of a few centuries is not persistent on longer time-scales. The smallest misfit between data and model is obtained, however, if a 3kyr average instead of a zero assumption is used as smoothing constraint. Distinct northern and southern hemisphere flux lobes are clearly compatible with the available data spanning the past 7kyrs. Note, however, that persistence in time averages of the field does not exclude significant temporal variations on shorter intervals; indeed, from the detailed temporal behaviour there is evidence for considerable variability in these features.

However, clever modelling can take us only so far. While we have demonstrated that currently available data do not preclude southern hemisphere flux patches, only by expanding the data base for this region can we truly determine the long-term morphology and variability of the southern hemisphere magnetic field.

Acknowledgements

We thank two anonymous reviewers who provided very constructive comments that improved the mansucript. Funding for RH and the collaboration which produced this research was provided by NERC grant NER/O/S/2003/00675. The project was completed with support of a DAAD travel grant.

References

Bloxham, J., Gubbins, D., 1987. Thermal core-mantle interactions. Nature 325, 511–513.

Bloxham, J., Gubbins, D., Jackson, A., 1989. Geomagnetic secular variation. Philos. Trans. R. Soc. London Ser. A 92, 415–502.

Bloxham, J., Jackson, A., 1992. Time-dependent mapping of the magnetic field at the core-mantle boundary. J. Geophys. Res. 97, 19,537–19,563.

Constable, C. G., Johnson, C. L., Lund, S. P., 2000. Global geomagnetic field models for the past 3000 years: transient or permanent flux lobes? Phil. Trans. R. Soc. Lond. A 358, 991–1008.

Davies, C. J., Gubbins, D., Willis, A. P., Jimack, P. K., 2008. Time-averaged paleomagnetic field and secular variation: Predictions from dynamo solutions based on lower mantle seismic tomography. Phys. Earth Planet. Int. 169, 194–203.

Donadini, F., Korte, M., Constable, C., 2009. Geomagnetic field for 0-3ka: 1. new data sets for global modeling. Geochem. Geophys. Geosys. 10, Q06007, doi:10.1029/2008GC002295.

Gubbins, D., 1975. Can the Earth's magnetic field be sustained by core oscillations? Geophys. Res. Lett. 2, 409–412.

Gubbins, D., 1987. Mechanism for geomagnetic polarity reversals. Nature 326, 167–169.

Gubbins, D., Bloxham, J., 1985. Geomagnetic field ananlysis - III. Magnetic fields on the core-mantle boundary. Geophys. J. R. Astron. Soc. 80, 695–713.

Holme, R., 2000. Electromagnetic core-mantle coupling III: laterally varying mantle conductance. Phys. Earth Planet. Int. 117, 329–344.

Jackson, A., 2003. Intense equatorial flux spots on the surface of the Earth's core. Nature 424, 760–763.

Jackson, A., Jonkers, A. R. T., Walker, M. R., 2000. Four centuries of geomagnetic secular variation from historical records. Phil. Trans. R. Soc. Lond. A 358, 957–990.

Johnson, C. L., Constable, C. G., 1995. The time-averaged geomagnetic field as recorded by lava flows over the past 5 Myr. Geophys. J. Int. 122, 489–519.

Johnson, C. L., Constable, C. G., 1997. The time-averaged geomagnetic field: global and regional biases for 0-5 Ma. Geophys. J. Int. 131, 643–666.

Jonkers, A. R. T., Jackson, A., Murray, A., 2003. Four centuries of geomagnetic data from historical records. Rev. Geophys. 41,2, doi:10.1029/2002RG000115.

Kelly, P., Gubbins, D., 1997. The geomagnetic field over the past 5 Myr. Geophys. J. Int. 128, 315–330.

Korte, M., Constable, C. G., 2005. Continuous geomagnetic field models for the past 7 millennia: 2. CALS7K. Geochem., Geophys., Geosys. 6, Q02H16, doi:10.1029/2004GC000801.

Korte, M., Constable, C. G., 2008. Spatial and temporal resolution of millennial scale geomagnetic field models. J. Adv. Space Res. 41, 57–69.

Korte, M., Donadini, F., Constable, C., 2009. Geomagnetic field for 0-3ka: 2. a new series of time-varying global models. Geochem. Geophys. Geosys. 10, Q06008, doi:10.1029/2008GC002297.

Korte, M., Genevey, A., Constable, C. G., Frank, U., Schnepp, E., 2005. Continuous geomagnetic field models for the past 7 millennia: 1. a new global data compilation. Geochem., Geophys., Geosys. 6, Q02H15, doi:10.1029/2004GC000800.

Lesur, V., Wardinski, I., Rother, M., Mandea, M., 2008. GRIMM: the GFZ Reference Internal Magnetic Model based on vector satellite and observatory data. Geophys. J. Int. 173, 382–394.

Macmillan, S., Maus, S., 2005. Modelling the Earth's magnetic field; the 10th generation IGRF. Earth, Planets, Space 57(12), 1135–1140.

McElhinny, M. W., Senanayake, W. E., 1982. Variations in the geomagnetic dipole: I. The past 50 000 years. J. Geomag. Geoelectr. 34, 39–51.

Mothersill, J. S., 1996. Paleomagnetic results from lakes Victoria and Albert, Uganda. Studia geoph. et geod. 40, 25–35.

Olsen, N., Mandea, M., Sabaka, T. J., Toffner-Clausen, L., 2009. CHAOS-2 – a geomagnetic field model derived from one decade of continuous satellite data. Geophys. J. Int. 179, 1477–1487.

Willis, A. P., Sreenivasan, B., Gubbins, D., 2007. Thermal core-mantle interaction: Exploring regimes for 'locked' dynamo action. Phys. Earth Planet. Int. 165, 83–92.

Yang, S., Odah, H., Shaw, J., 2000. Variations in the geomagnetic dipole moment over the last 12000 years. Geophys. J. Int. 140, 158–162.